Letter

Giant spin-selective bandgap renormalization in $CsPbBr_3$ colloidal nanocrystals

Megha Shrivastava,[1] Abhijit Hazarika,[2,3] J. Aneesh,[1] Dipendranath Mandal,[1] Matthew C. Beard,[2] and K. V. Adarsh[1,*]

[1]*Department of Physics, Indian Institute of Science Education and Research Bhopal, Bhopal 462066, India*

[2]*Chemistry & Nanoscience Center, National Renewable Energy Laboratory, Golden, Colorado 80401, United States*

[3]*Polymers and Functional Materials Division, CSIR-Indian Institute of Chemical Technology, Uppal Road, Tarnaka 500007, India*

(Received 21 April 2022; revised 14 June 2022; accepted 17 June 2022; published 5 July 2022)

The spin-dependence of the strongly correlated phenomena and many-body interactions play an important role in quantum information science. In particular, it is quite interesting but unclear how the spin degree of freedom ramifies the bandgap renormalization, one of the fundamental many-body phenomena. We report the first room-temperature observation of giant spin-selective bandgap renormalization (SS-BGR) in $CsPbBr_3$ colloidal nanocrystals using time-resolved circularly polarized femtosecond pump-probe spectroscopy. The SS-BGR results from many-body interactions among carriers with the same spin that renormalize their joint density of states by 57± 1 meV, visualized here as photoinduced absorption (PIA) below band-edge transition energy when the pump and probe are co-polarized. The hallmark result of spectrally resolved SS-BGR is in stark contrast to the usually submerged signal in II-VI and III-V semiconductors and is 3 orders of magnitude larger than that observed in Ge/SiGe quantum wells, highlighting the unique and beneficial band structure of the metal-halide semiconductors. We propose that the PIA, due to SS-BGR, can be used to describe the spin-polarization and spin-relaxation dynamics. The experimental and theoretical findings open up new possibilities for optical manipulation of spin degrees of freedom and their many-body interactions in metal-halide perovskite nanocrystals for potential room-temperature applications.

DOI: 10.1103/PhysRevB.106.L041404

Many-body interactions of charge carriers in quantum and spatially confined semiconducting nanostructures are enhanced relative to their bulk counterparts and thus have opened new opportunities for manipulating and enhancing light-matter interactions [1–5]. From a fundamental point of view, the enhanced Coulomb interactions due to the low-dimensional confinement endow carrier–carrier interactions, predicted to generate exotic effects such as exciton complexes [2,6–9], Mott transitions [4,10–12], bandgap renormalization (BGR) [4,13], charge density waves [14,15], and Bose-Einstein and Fermionic condensates [16,17]. Among these, BGR, a many-body effect described as a lowering of the fundamental bandgap with increasing free-carrier density [4,13], is of particular importance as it provides insight into the feasibility of utilizing nanostructures in various optoelectronic and photonic applications such as optical switches, saturable absorbers, and modulators [13].

Defect tolerant metal-halide perovskite nanocrystals (MHPN) of general formula ABX_3 are ideal candidates for studying above listed many-body phenomena arising from the interaction between charge carriers [18–25]. Here, A is a monovalent organic cation like methylammonium (MA) or formamidinium (FA), or an inorganic cation like Cesium (Cs); B is a divalent metal like Pb^{2+}, Sn^{2+}; and X is a halide ion like Cl^-, Br^-, and I^-. Likewise, in recent times, MHPN have been demonstrated to host novel spin functionalities [18,26–36]. Compared to conventional III-V and II-VI semiconductors [37,38], the valence band (VB) states of MHPN are formed from hybridization between B metal s orbitals and X halide p orbitals, while B metal p orbitals form the conduction band (CB) states [26,39]. The strong spin-orbit coupling (SOC) and the Rashba effect contribute to the ability to control the spin-properties of electrons, holes, and excitonic complexes via structural and/or compositional variation [26,27,40]. The MHPN have twofold degenerate CB minima and VB maxima, characterized by $|J, m_j\rangle = |\frac{1}{2}, \pm\frac{1}{2}\rangle$, where J and m_j represent the total angular momentum and magnetic quantum number [18,28,35,41], respectively; and the $J = 3/2$ CB manifold is split-off by ∼1 eV due to the large SOC leaving a simple two-level system at the band edge [41]. This two-level system provides clean spin-selection rules for optical transitions and thus the ability to optically prepare, manipulate, and measure the carrier spins and their populations. Recent demonstrations of striking spin functionalities in MHPN that have been at the forefront of development include long carrier spin coherence [29], size and composition dependent spin-relaxation [30], room-temperature spin-polarization via magnetic field effects [31], transient circular dichroism [28], Rashba effect leading to unique exciton fine structure [26,32,40], spin-polarized exciton-polaritons and condensates [33,42], and coherent optical Stark effect [27,34]. However, these studies largely ignored many-body interactions among carriers and thus, despite the flurry of parallel research, the correlation between the spin degree of freedom and many-body interactions in MHPN remains largely unexplored. Indeed, very recently, we established intervalley polaronic biexcitons of binding energy nearly equal to the exciton binding energy [36] and Floquet biexciton mediated coherent excitonic optical Stark effect in $CsPbBr_3$

*adarsh@iiserb.ac.in

nanocrystals [18]. These results were observed in thin films, mostly excitonic in nature, where spin-selective multi-exciton effects dominate the optical response. Having said that, the spin-selective bandgap renormalization effects are expected in the free-carrier system. Although bandgap renormalization is well established in MHPN [19,24,25], the spin-selective bandgap renormalization (SS-BGR) has neither been observed experimentally nor predicted theoretically. However, the SS-BGR is demonstrated in Ge/SiGe quantum wells and III-V and II-VI semiconductor single-crystals such as GaAs and CdTe [37,38,43,44]. But these samples require advanced fabrication techniques like molecular beam epitaxy and high-end single-crystal growth facility. At this point, it is important to mention that the SS-BGR observed in these samples is either submerged or partially offset by strong band-filling effects. Therefore, to date, the experimental demonstration of spectrally-resolved SS-BGR and its applications at room-temperature is completely missing.

Herein, we demonstrate the first experimental observation of spectrally resolved giant SS-BGR at room-temperature in a facile and cost-effective solution processed $CsPbBr_3$ colloidal nanocrystals using time-resolved circular-polarized pump-probe differential transient absorption spectroscopy. The exciton binding energy ~10 meV in our weakly confined nanocrystals indicate that the dynamics are mainly governed by the response of free-carriers. The giant SS-BGR ~57 meV is ~3 orders of magnitude larger than that in Ge/SiGe quantum wells where the magnitude of SS-BGR is ~0.006 meV at 10 K [43]. The SS-BGR in our case is exclusively demonstrated as a clear redshift of the joint density of states (continuum states) within one spin sub-band as per spin selection rules and visualized as a rapid emergence of a photoinduced absorption (PIA) below the band-edge transition energy for the co-polarized pump-probe condition. A pump-energy detuning study indicates an inverse scaling of the SS-BGR with increasing pump energy and loss of spin-selectivity for pump energies above the bandgap. Further, fluence dependent study shows the saturation of the SS-BGR shift with increasing pump-fluence. Our study opens up the potential to manipulate spin degrees of freedom and reveal crucial information on the unexplored spin-selective many-body interacting regime in MHPN, promoting their potential candidature for quantum information processing and opto-spintronic applications at room-temperature.

The ground state optical absorption (OA) spectrum of the $CsPbBr_3$ nanocrystals (synthesis details in the Supplemental material (SM) [45]), shown in Fig. 1, represent a sharp exciton onset at ~2.41 eV followed by the continuum absorption. These two contributions are separated by fitting the experimental data using the Elliott equation [19,25,46], details in SM [45]. By this method, we extracted the exciton (E_0) and bandgap continuum (E_{BG}) transitions that are centered at 2.42 ± 0.01 and 2.43 ± 0.01 eV, respectively. This renders the exciton binding energy to be 10 ± 1 meV, implying that the excitons are weakly bound, and as a result, free-carriers dominate the dynamics, similar to that observed for bulk MHP systems [25,47]. Figure 1 also describes the strong and narrow excitonic photoluminescence with full width at half maximum (FWHM) ~ 85 meV centered at 2.42 eV, confirming the high

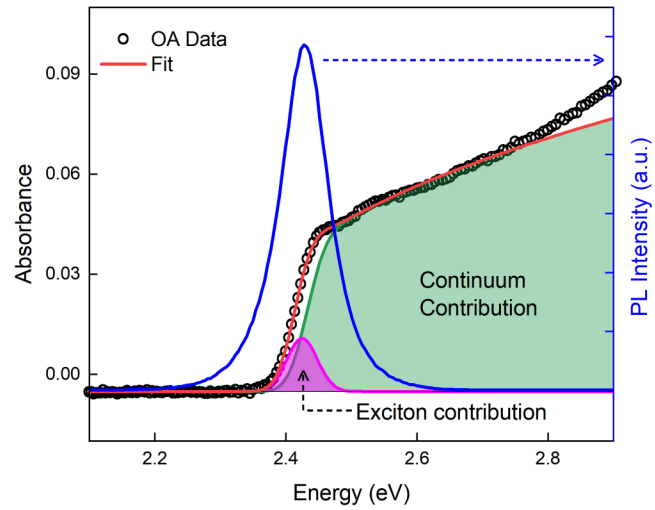

FIG. 1. Ground state OA spectrum together with theoretical fit using Elliott's model. The exciton absorption is centered at 2.42 eV, and the binding energy is 10 meV. Blue line is the photoluminescence spectrum which shows sharp exciton emission of FWHM 85 meV centered at 2.42 eV (at the exciton position obtained from Elliott's model).

quality as well as uniform dispersion of nanocrystals in the solutions.

We employed time-resolved circular-polarized pump-probe differential transient absorption spectroscopy to study the spin-selective many-body interactions. In our experiment, 100 fs pump pulses (tunable from 2.29-2.48 eV) derived from an optical parametric amplifier was used to excite the sample. The differential absorption (ΔA), defined as the difference in absorption of the white-light continuum probe (spanning energies from 2.2-2.6 eV) in the excited and ground state, is measured for co-polarization [σ^+ pump - σ^+ probe ($\sigma^+\sigma^+$)] and counter-polarization ($\sigma^+\sigma^-$) configurations (see SM [45] and Fig. S1). Figures 2(a) and 2(b) presents $\sigma^+\sigma^+$ and $\sigma^+\sigma^-$ pseudocolor ΔA spectrum and corresponding

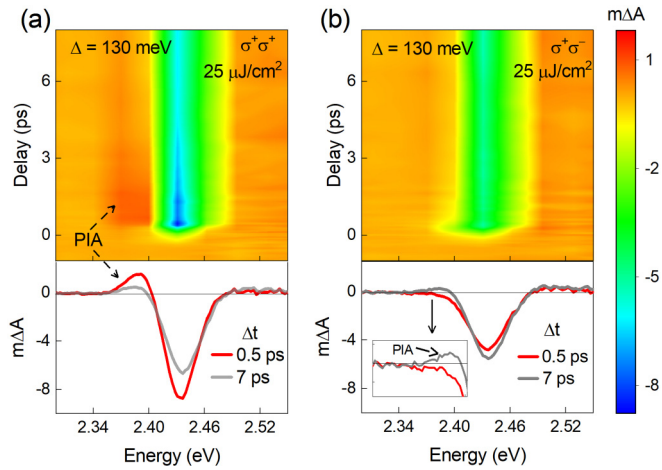

FIG. 2. The pseudocolor ΔA spectrum of $CsPbBr_3$ nanocrystals for $\Delta = 130$ meV at a fixed pump fluence of 25 $\mu J/cm^2$, for (a) $\sigma^+\sigma^+$ and (b) $\sigma^+\sigma^-$. The corresponding cross-sections at pump-probe delay time (Δt) of 0.5 and 7 ps are shown in the bottom panel. The inset in (b) shows the zoomed-in image of the PIA.

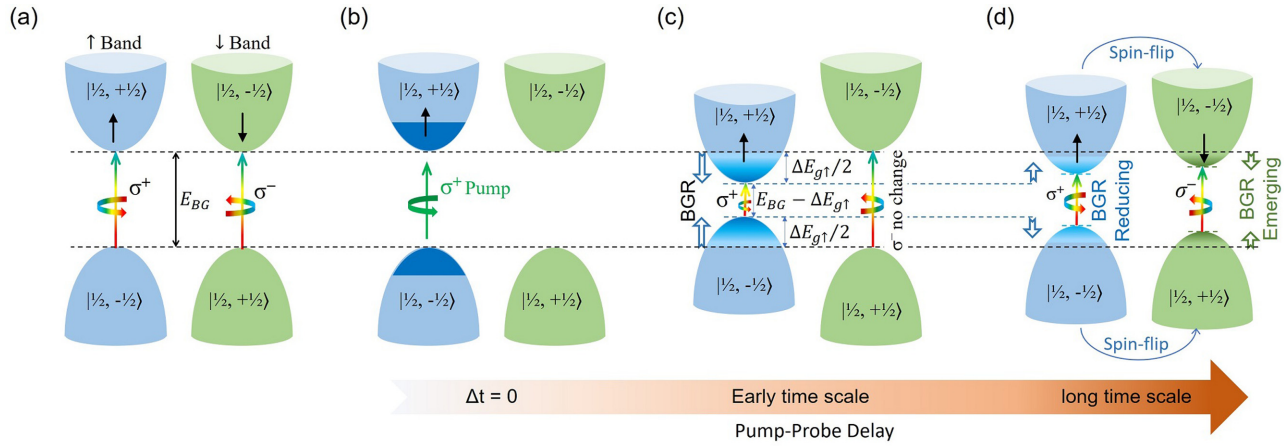

FIG. 3. (a) Illustration of the optical selection rules: σ^+ polarized probe monitors the change in ↑ band, i.e., change in the transition from $|\frac{1}{2}, -\frac{1}{2}\rangle$ VB to $|\frac{1}{2}, +\frac{1}{2}\rangle$ CB, while σ^- polarized probe monitors the change in ↓ band, i.e., transition from $|\frac{1}{2}, +\frac{1}{2}\rangle$ VB to $|\frac{1}{2}, -\frac{1}{2}\rangle$ CB. The black up and down arrows manifest the angular momentum orientation of the electrons. (b) Population of the ↑ band (dark blue region) by σ^+ pump pulse as per the optical selection rules. (c) The renormalization of the ↑ band due to interactions among spin-carriers in ↑ band and no shift in ↓ band since the band is empty at early time scale. (d) Spin-flipping of carriers from ↑ band to ↓ band and the corresponding decay of BGR in ↑ band with simultaneous growth in ↓ band, providing the direct evidence of spin-selective BGR.

cross-sections at $\Delta t = 0.5$ and 7 ps, for a pump detuning energy (Δ) of 130 meV and a fluence of 25 $\mu J/cm^2$; here the detuning is defined as $\Delta = E_{BG}$-$\hbar\omega$, where $\hbar\omega$ is pump photon energy, such that positive detuning corresponds to pump photon energies that are below the bandgap.

Strikingly, the $\sigma^+\sigma^+$ ΔA spectrum manifests an unusual and unprecedented PIA below the band-edge in addition to the strong bleach at the exciton position. In contrast, there is no PIA signal observed at early times ($\Delta t = 0.5$ ps) for the $\sigma^+\sigma^-$ but rather shows a weaker bleach at the excitonic position due to state-filling. The observation of PIA under $\sigma^+\sigma^+$ is in contrast with previous reports and conventions observed to date [6,7,18,27,28,34,36,41,48–50]. For instance, $\sigma^+\sigma^+$ pump-probe conditions can lead to a coherent optical Stark shift that exhibits a blue-shifted excitonic absorption and only exists for the pump pulse duration [7,18,27,34,49,50]. In contrast, the PIA that we observed here indicates a red-shifted absorption and exists for two-orders of magnitude longer than the pump-pulse duration, thus we can rule out the optical Stark-shift as the origin of these observations. In addition, we can discount the biexciton as the origin of PIA based on spin-selection rules [2,6,7,9,18,36] and the small exciton binding energy of ∼10 meV. A biexciton, created by the probe pulse, would result in a red-shifted PIA but only for the case of counter polarization (i.e., $\sigma^+\sigma^-$) and not for the co-polarization conditions. We also disregard trion [9] formation as the source of these observations for the same reason.

To decipher the hallmark results observed here, we turn to the predictions of the well-developed many-body theory for semiconductors [51], which is largely ignored and overlooked in describing spin functionalities in MHPN [27,29,31,33]. Based on the many-body theory of charge carriers and spin-selection rules, we assign the spin-selective PIA to SS-BGR. Such SS-BGR effect is known to occur in Ge/SiGe quantum wells [43], II-VI [37], and III-V [38,44], bulk semiconductors. However, our results are compelling because the SS-BGR signal in those reported results is usually submerged or partially offset by strong band-filling effects. In contrast, the emergence of the PIA signal in our case exclusively demonstrates a clear spectrally resolved SS-BGR at room-temperature. The SS-BGR originates from screening of the repulsive Coulomb interactions between the photogenerated carriers of the same sign that results in a redshift [13,52–54]. Figure 3(a) illustrates the optical selection rules that allow transitions for $\Delta J = 0$ and $\Delta m_j = \pm 1$. The σ^+ (σ^-) probe carrying an angular momentum of +1 (1) selectively initializes the transition from $|\frac{1}{2}, -\frac{1}{2}\rangle$ ($|\frac{1}{2}, +\frac{1}{2}\rangle$) VB to $|\frac{1}{2}, +\frac{1}{2}\rangle$ ($|\frac{1}{2}, -\frac{1}{2}\rangle$) CB which we denote here as ↑ (↓) band for simplicity, blue (green) parabolas. The σ^+ pump photons, as per the spin-selection rules, optically initialize electrons in the ↑ band, Fig. 3(b).

Soon after the absorption of the pump pulse, the reduction of the repulsive Coulomb interaction among photogenerated carriers in ↑ VB and CB result in renormalization, which is monitored by σ^+ probe, Fig. 3(c). On the other hand, ↓ band does not encounter any such renormalization since this band is empty at an early time. Thus, the action of photoexcitation along with the SS-BGR lifts the degeneracy of the ↑, ↓ spin levels at the band edges. This can also be noticed from the emergence of PIA only in $\sigma^+\sigma^+$ and absence in $\sigma^+\sigma^-$ at $\Delta t = 0.5$ ps, in Figs. 2(a) and 2(b) bottom panel. Now, as time progresses, the carriers in ↑ band undergo a spin-flip and populate ↓ band in Fig. 3(d), leading to the decay of the PIA in the σ^+ probe and a simultaneous rise of a PIA in the σ^- probe, Figs. 2(a) and 2(b)bottom panel, and Fig. S2. The simultaneous decay and growth of PIA in ↑ and ↓ bands, respectively, were used to calculate the spin-polarization lifetime of ∼2.5 ps (Fig. S2) in stark contrast to the previous reports considering a non-interacting framework [30,35,55,56], details in SM [45] and Fig. S3. The ΔA spectra at $\Delta t = 7$ ps shown in Figs. 2(a) and 2(a) bottom panel manifest the PIA for both $\sigma^+\sigma^+$ and $\sigma^+\sigma^-$ configuration, in excellent accordance with the explanation above. Overall, our experimental results provide the direct evidence of spectrally well resolved SS-BGR at room-temperature in $CsPbBr_3$ colloidal nanocrystals.

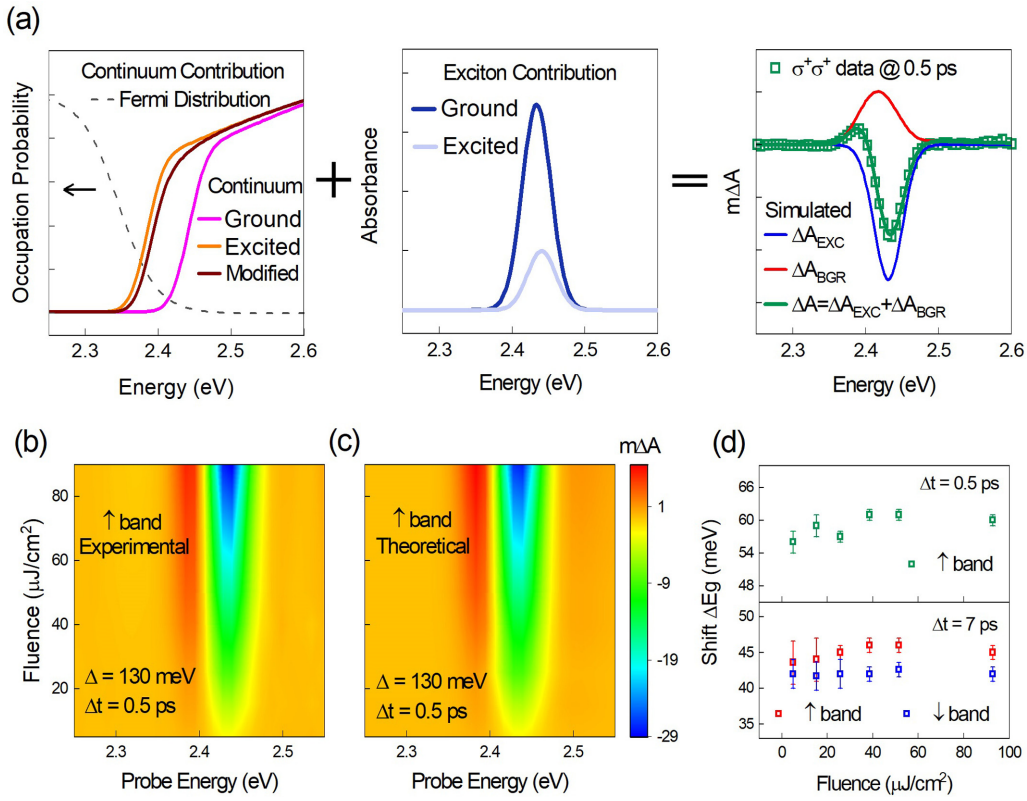

FIG. 4. (a) The leftmost panel shows the continuum in the Excited state (orange) and Ground state (magenta) and the modified (wine) continuum states as per the Fermi-distribution function (black dashed line). Middle panel shows the exciton bleach by free-carriers. The rightmost panel shows the simulated ΔA (green) from the combined effect of SS-BGR (red) and exciton bleach (blue). The symbols present the experimental ΔA for ↑ band at $\Delta t = 0.5$ ps (for $\Delta = 130$ meV, pump fluence 25 μJ/cm^2) that is in agreement with our model. (b), (c) Pseudocolor plot of ΔA (b) experimental and (c) modeled corresponding to ↑ band at $\Delta t = 0.5$ ps as a function of fluence at constant $\Delta = 130$ meV; (d) The JDOS shift evaluated using Eqs. (1)–(3) at different fluence exhibiting saturation at $\Delta t = 0.5$ ps for ↑ band (top panel) and $\Delta t = 7$ ps for ↑ band and ↓ band (bottom panel).

To quantitatively analyze the SS-BGR, we model the ΔA spectrum at 0.5 ps (before spins depolarize) for ↑ band and 7 ps (after spins depolarize) for ↑ and ↓ bands using

$$\Delta A(E,t) = \Delta A_{\mathrm{EXC}}(E,t) + \Delta A_{\mathrm{BGR}}(E,t), \tag{1}$$

$$\Delta A_{\mathrm{EXC}}(E,t) = \left(BA_g e^{\left(\frac{E-E_{0_e}}{\Gamma}\right)^2} - A_g e^{\left(\frac{E-E_{0_g}}{\Gamma}\right)^2}\right), \tag{2}$$

$$\Delta A_{\mathrm{BGR}}(E,t) = \left(A_{c_e}(E;E_{\mathrm{BG}} - \Delta E_g^{\uparrow(\downarrow)},\Gamma)\left[1 - f_e^{q\uparrow(\downarrow)}\left(E;E_f^{q\uparrow(\downarrow)},T_c\right)\right]^2\right) - A_{c_g}(E;E_{\mathrm{BG}},\Gamma), \tag{3}$$

where B, A_g, Γ, $\Delta E_g^{(\uparrow(\downarrow))}$, $E_f^{(q\uparrow(\downarrow))}$, $f_e^{(q\uparrow(\downarrow))}$, T_c, and A_c refer to oscillator strength, amplitude of band-edge transition, FWHM, shift of the ↑ (↓) band due to SS-BGR, quasifermi energy within the ↑ (↓) band, fermi distribution function, carrier temperature (300 K) and continuum contribution. The subscripts e and g denote the excited and ground state, respectively. The ΔA_{BGR} and ΔA_{EXC} refer to the change in ΔA spectra due to SS-BGR and change in exciton absorption. The pump beam result in photogenerated carriers that follows fermi-Dirac distribution characterized by fermi energy E_f^q [19,25,35], is shown by black dashed line, Fig. 4(a) leftmost panel. The photogenerated carriers screen the Coulombic interactions [13,52], resulting in the red-shift of the continuum transition (orange curve), thereby renormalizing the bandgap and leading to the absorption of probe corresponding to the modified continuum states (wine curve), quantified by curly bracket term in Eq. (3).

In addition to the SS-BGR, the change in absorption of exciton transition due to state filling [19,57] and reduction in exciton binding energy due to screened attractive Coulombic interactions [13,52,53] (illustrated in Fig. 4(a) middle panel) also modulates the ΔA spectrum. The combined effect of the changes contributed by SS-BGR and exciton results in a derivative feature (green-trace), shown in Fig. 4(a), rightmost panel. The symbols represent the experimental data which is in agreement with the simulations performed using our phenomenological model. The simulation of the cross-section spectra at $\Delta t = 0.5$ ps (for ↑ band) using Eqs. (1)–(3) reveal renormalization by as much as 57 ± 1 meV. The $\Delta E_g^{[\uparrow(\downarrow)]}$ (shift due to SS-BGR) decreases (increases) to 45 ± 3 (42 ± 2) meV at 7 ps for ↑ (↓) band, providing direct evidence for our intuitive model (Fig. 3). The giant SS-BGR shift we observed at room-temperature is three orders of magnitude larger than that reported in Ge/SiGe quantum wells at cryogenic temperature [43].

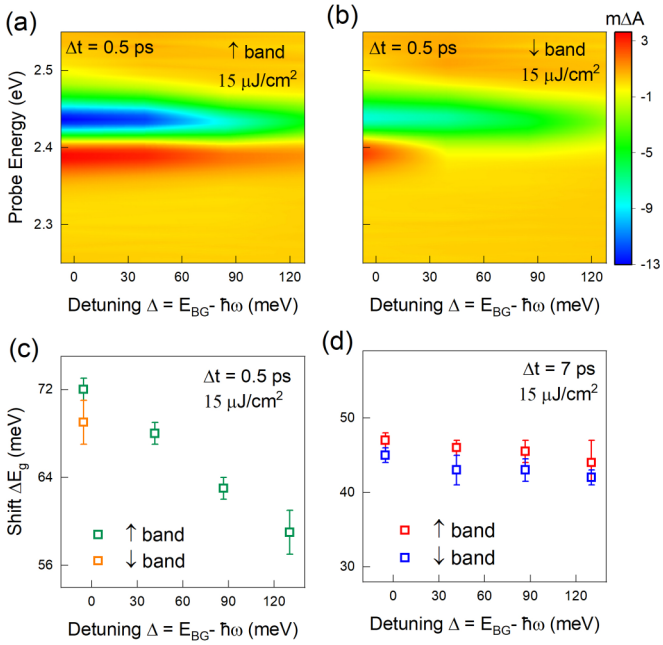

FIG. 5. (a), (b) Pseudocolor plot of ΔA at 0.5 ps as a function of Δ at constant fluence of 15 $\mu J/cm^2$ for (a) ↑ band and (b) ↓ band. (c), (d) The BGR shift evaluated using Eqs. (1)–(3) at different Δ for ↑ band and ↓ band at (c) $\Delta t = 0.5$ ps and (d) $\Delta t = 7$ ps.

To have a complete picture of the SS-BGR, we carried out fluence dependent study both experimentally and numerically. Figure 4(b) presents the experimentally recorded fluence dependent ΔA spectrum at $\Delta t = 0.5$ ps for ↑ band. The numerically simulated spectrum using Eqs. (1)–(3), shown in Fig. 4(c) is found to be in excellent agreement with the experimental data, which further validates our phenomenological model of SS-BGR. Noticeably, the ΔE_g at $\Delta t = 0.5$ ps for ↑ band and $\Delta t = 7$ ps for ↑ and ↓ band [Fig. 4(d)] exhibit saturation, in contrast to the expected cube-root dependence [13,38,58]. This can be understood by considering the fact that in conventional semiconductors above the Mott density [10,13], all the excitons in the system ionize to free-carriers, and above this threshold, the saturation of BGR can occur. As already noted, $CsPbBr_3$ nanocrystals here are already in a free-carrier regime, so the BGR saturation can be expected even at low fluences. The spin polarization lifetime as a function of fluence is shown in Fig. S4.

After demonstrating the SS-BGR at a fixed Δ, the ΔA in ↑ and ↓ bands were systematically measured by continuously varying the pump photon energy, thereby Δ, and presented in Figs. 5(a) and 5(b) at $\Delta t = 0.5$ ps. Figure 5(a) and 5(c) manifest that the amplitude and $\Delta E_g^{\uparrow}$ increase significantly with a decrease in Δ for ↑ band. The $\Delta E_g^{\uparrow}$ becomes as much as ∼72 meV for $\Delta < 0$. Importantly for ↓ band, there is no SS-BGR for larger Δ, however, this picture changes dramatically when $\Delta < 0$ [Fig. 5(b) and 5(d)]. In this case, the BGR response occurs even in the ↓ band, i.e., the spin selectivity of the BGR is completely lost for the above bandgap excitation. The loss of spin polarization accelerates with a decrease in detuning (Fig. S5), and for the above bandgap excitation, it is less than our experimental window resolution. Spin-depolarization can increase when the carriers have excess energy due to rapid phonon emission via the Elliot-Yafet mechanism [59,60]. Therefore, due to the rapid spin-flip, both ↑ and ↓ bands are populated, and the loss of spin-selectivity of BGR is apparent.

In conclusion, we demonstrated the first room-temperature experimental observation of well-resolved giant SS-BGR as the emergence of PIA below band-edge transition. The numerical simulations performed using a phenomenological model of SS-BGR well describes all important experimentally observed features. Our findings offer a foundation for the SS-BGR at room-temperature in perovskite nanocrystals, and our model can even be applied to other semiconductors. These studies provide crucial information on the unexplored spin-dependent many-body interactions and pave the way for the potential generation and manipulation of the quantum spin of carriers and their complexes at room-temperature for an all-optical controlled ultrafast switching and highly correlated quantum phenomena such as quantum droplets and quantum information processing.

The authors gratefully acknowledge the Science and Engineering Research Board (Project No. CRG/2019/002808) and DST-FIST Project (PSI-195/2014) for Department of Physics. K.V.A. gratefully acknowledges the DST-IUSSTF BASE fellowship. This work was supported in part by the National Renewable Energy Laboratory (NREL), operated by Alliance for Sustainable Energy LLC, for the U.S. Department of Energy (DOE) under contract No. DE-AC36-08GO28308. Work at NREL was supported as part of the Centre for Hybrid Organic Inorganic Semiconductors for Energy (CHOISE) an Energy Frontier Research Centre funded through the Office of Basic Energy Sciences, Office of Science within the U.S. DOE. The views expressed in this article do not necessarily represent the views of the DOE or the U.S. Government.

[1] J. Shah, M. Combescot, and A. H. Dayem, Phys. Rev. Lett. **38**, 1497 (1977).
[2] E. J. Sie, A. J. Frenzel, Y. H. Lee, J. Kong, and N. Gedik, Phys. Rev. B **92**, 125417 (2015).
[3] D. S. Chemla and J. Shah, Nature (London) **411**, 549 (2001).
[4] S. K. Bera, M. Shrivastava, K. Bramhachari, H. Zhang, A. K. Poonia, D. Mandal, E. M. Miller, M. C. Beard, A. Agarwal, and K. V. Adarsh, Phys. Rev. B **104**, L201404 (2021).
[5] W. Yu, Z. Dong, I. Abdelwahab, X. Zhao, J. Shi, Y. Shao, J. Li, X. Hu, R. Li, T. Ma, Z. Wang, Q. H. Xu, D. Y. Tang, Y. Song, and K. P. Loh, ACS Nano **15**, 18448 (2021).
[6] E. J. Sie, C. H. Lui, Y.-H. Lee, J. Kong, and N. Gedik, Nano Lett. **16**, 7421 (2016).
[7] C. K. Yong, J. Horng, Y. Shen, H. Cai, A. Wang, C. S. Yang, C. K. Lin, S. Zhao, K. Watanabe, T. Taniguchi, S. Tongay, and F. Wang, Nat. Phys. **14**, 1092 (2018).

[8] P. Taank, R. Karmakar, R. Sharma, R. K. Yadav, M. Shrivastava, N. C. Maurya, T. K. Maji, D. Karmakar, and K. V. Adarsh, J. Phys. Chem. C **126**, 416 (2022).

[9] A. Steinhoff, M. Florian, A. Singh, K. Tran, M. Kolarczik, S. Helmrich, A. W. Achtstein, U. Woggon, N. Owschimikow, F. Jahnke, and X. Li, Nat. Phys. **14**, 1199 (2018).

[10] A. Steinhoff, M. Florian, M. Rösner, G. Schönhoff, T. O. Wehling, and F. Jahnke, Nat. Commun. **8**, 1166 (2017).

[11] M. Stern, V. Garmider, V. Umansky, and I. Bar-Joseph, Phys. Rev. Lett. **100**, 256402 (2008).

[12] A. Chernikov, A. M. van der Zande, H. M. Hill, A. F. Rigosi, A. Velauthapillai, J. Hone, and T. F. Heinz, Phys. Rev. Lett. **115**, 126802 (2015).

[13] A. Chernikov, C. Ruppert, H. M. Hill, A. F. Rigosi, and T. F. Heinz, Nat. Photonics **9**, 466 (2015).

[14] P. Dreher, W. Wan, A. Chikina, M. Bianchi, H. Guo, R. Harsh, S. Mañas-Valero, E. Coronado, A. J. Martínez-Galera, P. Hofmann, J. A. Miwa, and M. M. Ugeda, ACS Nano **15**, 19430 (2021).

[15] Y. Chen, L. Wu, H. Xu, C. Cong, S. Li, S. Feng, H. Zhang, C. Zou, J. Shang, S. A. Yang, K. P. Loh, W. Huang, and T. Yu, Adv. Mater. **32**, 2003746 (2020).

[16] Z. G. Koinov, Phys. Rev. B **61**, 8411 (2000).

[17] V. P. Kochereshko, M. V. Durnev, L. Besombes, H. Mariette, V. F. Sapega, A. Askitopoulos, I. G. Savenko, T. C. H. Liew, I. A. Shelykh, A. V. Platonov, S. I. Tsintzos, Z. Hatzopoulos, P. G. Savvidis, V. K. Kalevich, M. M. Afanasiev, V. A. Lukoshkin, C. Schneider, M. Amthor, C. Metzger, M. Kamp, S. Hoefling, P. Lagoudakis, and A. Kavokin, Sci. Rep. **6**, 20091 (2016).

[18] M. Shrivastava, F. Krieg, D. Mandal, A. K. Poonia, S. K. Bera, M. V. Kovalenko, and K. V. Adarsh, Nano Lett. **22**, 808 (2022).

[19] A. Mondal, J. Aneesh, V. Kumar Ravi, R. Sharma, W. J. Mir, M. C. Beard, A. Nag, and K. V. Adarsh, Phys. Rev. B **98**, 115418 (2018).

[20] S. Bera and N. Pradhan, ACS Energy Lett. **5**, 2858 (2020).

[21] J. Aneesh, A. Swarnkar, V. Kumar Ravi, R. Sharma, A. Nag, and K. V. Adarsh, J. Phys. Chem. C **121**, 4734 (2017).

[22] K. E. Shulenberger, M. N. Ashner, S. K. Ha, F. Krieg, M. v. Kovalenko, W. A. Tisdale, and M. G. Bawendi, J. Phys. Chem. Lett. **10**, 5680 (2019).

[23] A. Dey, J. Ye, A. De, E. Debroye, S. K. Ha, E. Bladt, A. S. Kshirsagar, Z. Wang, J. Yin, Y. Wang, L. N. Quan, F. Yan, M. Gao, X. Li, J. Shamsi, T. Debnath, M. Cao, M. A. Scheel, S. Kumar, J. A. Steele, M. Gerhard, L. Chouhan, K. Xu, X. G. Wu, Y. Li, Y. Zhang, A. Dutta, C. Han, I. Vincon, A. L. Rogach, A. Nag, A. Samanta, B. A. Korgel, C. J. Shih, D. R. Gamelin, D. H. Son, H. Zeng, H. Zhong, H. Sun, H. V. Demir, I. G. Scheblykin, I. Mora-Seró, J. K. Stolarczyk, J. Z. Zhang, J. Feldmann, J. Hofkens, J. M. Luther, J. Pérez-Prieto, L. Li, L. Manna, M. I. Bodnarchuk, M. V. Kovalenko, M. B. J. Roeffaers, N. Pradhan, O. F. Mohammed, O. M. Bakr, P. Yang, P. Müller-Buschbaum, P. V. Kamat, Q. Bao, Q. Zhang, R. Krahne, R. E. Galian, S. D. Stranks, S. Bals, V. Biju, W. A. Tisdale, Y. Yan, R. L. Z. Hoye, and L. Polavarapu, ACS Nano **15**, 10775 (2021).

[24] R. Saran, A. Heuer-Jungemann, A. G. Kanaras, and R. J. Curry, Adv. Opt. Mater. **5**, 1700231 (2017).

[25] Y. Yang, D. P. Ostrowski, R. M. France, K. Zhu, J. van de Lagemaat, J. M. Luther, and M. C. Beard, Nat. Photonics **10**, 53 (2016).

[26] M. A. Becker, R. Vaxenburg, G. Nedelcu, P. C. Sercel, A. Shabaev, M. J. Mehl, J. G. Michopoulos, S. G. Lambrakos, N. Bernstein, J. L. Lyons, T. Stöferle, R. F. Mahrt, M. V. Kovalenko, D. J. Norris, G. Rainò, and A. L. Efros, Nature (London) **553**, 189 (2018).

[27] Y. Li, S. He, X. Luo, X. Lu, and K. Wu, J. Phys. Chem. Lett. **11**, 3594 (2020).

[28] W. Zhao, R. Su, Y. Huang, J. Wu, C. F. Fong, J. Feng, and Q. Xiong, Nat. Commun. **11**, 5665 (2020).

[29] V. V. Belykh, D. R. Yakovlev, M. M. Glazov, P. S. Grigoryev, M. Hussain, J. Rautert, D. N. Dirin, M. V. Kovalenko, and M. Bayer, Nat. Commun. **10**, 673 (2019).

[30] Y. Li, X. Luo, Y. Liu, X. Lu, and K. Wu, ACS Energy Lett. **5**, 1701 (2020).

[31] K. Zhang, J. Zhao, Q. Hu, S. Yang, X. Zhu, Y. Zhang, R. Huang, Y. Ma, Z. Wang, Z. Ouyang, J. Han, Y. Han, J. Tang, W. Tong, L. Zhang, T. Zhai, K. Zhang, J. Zhao, Y. Zhang, R. Huang, Y. Ma, Z. Wang, Z. Ouyang, J. Han, Y. Han, Q. Hu, J. Tang, S. Yang, T. Zhai, X. Zhu, W. Tong, and L. Zhang, Adv. Mater. **33**, 2008225 (2021).

[32] P. Tamarat, M. I. Bodnarchuk, J. B. Trebbia, R. Erni, M. V. Kovalenko, J. Even, and B. Lounis, Nat. Mater. **18**, 717 (2019).

[33] M. S. Spencer, Y. Fu, A. P. Schlaus, D. Hwang, Y. Dai, M. D. Smith, D. R. Gamelin, and X.-Y. Zhu, Sci. Adv. **7**, eabj7667 (2021).

[34] Y. Yang, M. Yang, K. Zhu, J. C. Johnson, J. J. Berry, J. Van De Lagemaat, and M. C. Beard, Nat. Commun. **7**, 12613 (2016).

[35] M. Shrivastava, M. I. Bodnarchuk, A. Hazarika, J. M. Luther, M. C. Beard, M. V. Kovalenko, and K. V. Adarsh, Adv. Opt. Mater. **8**, 2001016 (2020).

[36] A. K. Poonia, M. Shrivastava, W. J. Mir, J. Aneesh, A. Nag, and K. V. Adarsh, Phys. Rev. B **104**, L161407 (2021).

[37] P. Horodyská, P. Němec, T. Novotný, F. Trojánek, and P. Malý, J. Appl. Phys. **116**, 053913 (2014).

[38] P. Nemec, Y. Kerachian, H. M. van Driel, and A. L. Smirl, Phys. Rev. B **72**, 245202 (2005).

[39] J. Kang and L. W. Wang, J. Phys. Chem. Lett. **8**, 489 (2017).

[40] M. Isarov, L. Z. Tan, M. I. Bodnarchuk, M. V. Kovalenko, A. M. Rappe, and E. Lifshitz, Nano Lett. **17**, 5020 (2017).

[41] G. Yumoto, H. Hirori, F. Sekiguchi, R. Sato, M. Saruyama, T. Teranishi, and Y. Kanemitsu, Nat. Commun. **12**, 3026 (2021).

[42] R. Su, J. Wang, J. Zhao, J. Xing, W. Zhao, C. Diederichs, T. C. H. Liew, and Q. Xiong, Sci. Adv. **4**, eaau0244 (2018).

[43] C. Lange, G. Isella, D. Chrastina, F. Pezzoli, N. S. Köster, R. Woscholski, and S. Chatterjee, Phys. Rev. B **85**, 241303(R) (2012).

[44] Y. Chen, H. Lu, and T. Lai, J. Appl. Phys. **128**, 115704 (2020).

[45] See Supplemental Material at http://link.aps.org/supplemental/10.1103/PhysRevB.106.L041404 for the details on synthesis, time-resolved circular-polarizaed pump-probe differential absorption spectroscopy, exciton binding energy calculation using Elliott model, spin polarization lifetime calculations, fluence dependent spin polarization lifetime, detuning energy dependent spin polarization lifetime.

[46] R. J. Elliott, Phys. Rev. **108**, 1384 (1957).
[47] J. S. Manser and P. V. Kamat, Nat. Photonics **8**, 737 (2014).
[48] P. D. Cunningham, A. T. Hanbicki, T. L. Reinecke, K. M. McCreary, and B. T. Jonker, Nat. Commun. **10**, 5539 (2019).
[49] E. J. Sie, J. W. McLver, Y. H. Lee, L. Fu, J. Kong, and N. Gedik, Nat. Mater. **14**, 290 (2015).
[50] D. Giovanni, W. K. Chong, H. A. Dewi, K. Thirumal, I. Neogi, R. Ramesh, S. Mhaisalkar, N. Mathews, and T. C. Sum, Sci. Adv. **2**, e1600477 (2016).
[51] M. Kira and S. W. Koch, *Semiconductor Quantum Optics* (Cambridge University Press, Cambridge, England, 2011).
[52] M. M. Ugeda, A. J. Bradley, S.-F. Shi, F. H. da Jornada, Y. Zhang, D. Y. Qiu, W. Ruan, S.-K. Mo, Z. Hussain, Z.-X. Shen, F. Wang, S. G. Louie, and M. F. Crommie, Nat. Mater. **13**, 1091 (2014).
[53] E. J. Sie, A. Steinhoff, C. Gies, C. H. Lui, Q. Ma, M. Rösner, G. Schönhoff, F. Jahnke, T. O. Wehling, Y. H. Lee, J. Kong, and P. Jarillo-Herrero, Nano Lett. **17**, 4210 (2017).
[54] A. K. Nowak, E. Gallardo, H. P. van der Meulen, J. M. Calleja, J. M. Ripalda, L. González, and Y. González, Phys. Rev. B **83**, 245447 (2011).
[55] M. Zhou, J. S. Sarmiento, C. Fei, X. Zhang, and H. Wang, J. Phys. Chem. Lett. **11**, 1502 (2020).
[56] D. Giovanni, H. Ma, J. Chua, M. Grätzel, R. Ramesh, S. Mhaisalkar, N. Mathews, and T. C. Sum, Nano Lett. **15**, 1553 (2015).
[57] H. Zhu, M. T. Trinh, J. Wang, Y. Fu, P. P. Joshi, K. Miyata, S. Jin, and X.-Y. Zhu, Adv. Mater. **29**, 1603072 (2017).
[58] Z. M. Gibbs, A. Lalonde, and G. J. Snyder, New J. Phys. **15**, 075020 (2013).
[59] S. Strohmair, A. Dey, Y. Tong, L. Polavarapu, B. J. Bohn, and J. Feldmann, Nano Lett. **20**, 4724 (2020).
[60] W. Tao, Q. Zhou, and H. Zhu, Sci. Adv. **6**, eabb7132 (2020).